Design and Analysis of a Wideband 15–35-GHz Quadrature Phase Shifter With Inductive Loading

Suman P. Sah, *Student Member, IEEE*, Xinmin Yu, *Student Member, IEEE*, and Deukhyoun Heo, *Senior Member, IEEE*

***Abstract*—A Ku-, K-, and Ka-band phase shifter for beamforming applications is presented in this paper. An analysis showing the effect of loading conditions on quadrature phase accuracy in a simple poly-phase filter is carried out. Based on the analysis, a novel quadrature phase shifter (QPS) with inductive load is proposed. Sign-selection and vector addition is performed in two stages to lower supply voltage. The proposed phase shifter is fabricated in a 0.18-μm SiGe BiCMOS process and occupies an area of 520 μm $\times$ 370 μm. The proposed QPS has a maximum phase error of 6.38° over 15–35 GHz while maintaining an amplitude imbalance less than 2 dB. When combined into a 4-bit phase shifter, the root mean square (rms) gain error is less than 2.2 dB and the rms phase error is less than 13° over 15–35 GHz. The phase shifter thus achieves a full 360° phase-shift range with 22.5° phase resolution. The total power consumption is 14 mA from a 1.8-V power supply. The phase shifter achieves an input P1dB of −6.25 dBm. The measured phase-shifting fractional bandwidth of 87% is the highest reported thus far in the literature for SiGe BiCMOS implementation.**

***Index Terms*—All-pass filter, beamformer, BiCMOS, phase shifters, phased arrays, polyphase filter, quadrature filter.**

I. Introduction

A WIDEBAND RF front-end is essential in multi-band beamformer designs. Whereas many techniques to achieve wide-bandwidth in amplifiers exist in the literature [1], the lack of wideband phase shifters has limited the design of an ultra-wideband phased-array frontend. Quadrature phase shifters (QPSs) are essential building blocks for a phase shifter in a phased array. They are extensively used to generate basis quadrature vectors, which are then combined in an active or passive method to create required phase shifts. A QPS with high quadrature accuracy and low insertion loss over a wide bandwidth is extremely desirable for a wideband RF phase-shifting phased array. Quadrature phase-shift in the RF path can be implemented based on couplers [2]–[6], transmission lines [7], [8], LC circuits [9]–[13], delay line [14], and poly-phase filters (PPFs) [15]–[21]. Implementations using couplers, transmission lines, and variable delay lines are inherently narrowband and occupy a large area as well. LC circuits are small in size, but are narrowband. PPFs provide a relatively wide phase-shifting bandwidth with acceptable attenuation.

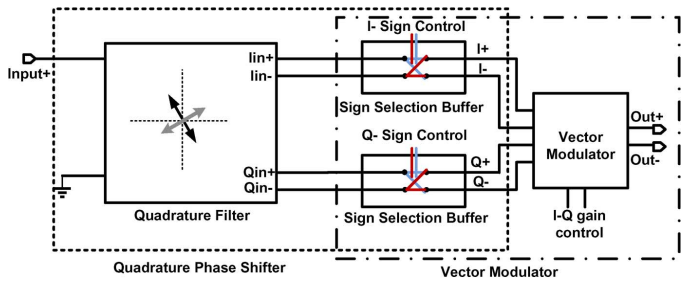

Fig. 1. Block diagram of the proposed wideband phase shifter.

PPFs are implemented in several forms of which all-pass filters [16]–[18] deserve proper attention, as they can achieve very low insertion loss while providing wideband quadrature outputs. However, the phase accuracy of such a filter is heavily dependent on output loading conditions [16]. The sensitivity of phase accuracy on loading conditions can be reduced by decreasing the Q of the filter [22]. Nevertheless, the problem of capacitive loading being comparable to the filter capacitance and variations in the load at different phase states still remains unsolved.

In this paper, a wideband Ku-, K-, and Ka-band phase shifter (Fig. 1) based on a novel polyphase quadrature filter is presented. A simple PPF is analyzed with respect to the effects of loading conditions in Section II. The presented analysis takes into account a general loading condition for the PPF in contrast to a capacitive-only loading, as considered in [22]. We then propose our QPS design in Section III. To verify the functionality of the QPS under practical loading conditions, a vector sum phase shifter implemented based on the proposed QPS is presented in Section IV. Section V provides measurement results, followed by concluding remarks in Section VI.

II. PPF Under Loading

A simple PPF with added load (Z_L) is shown in Fig. 2. Z_L can be expressed as $Z_L = r_L + jx_L$, where x_L is a function of frequency(ω). The transfer functions between $H_q(\omega) = V_q/V_{\text{in}}$ and $H_i(\omega) = V_i/V_{\text{in}}$ can now be written as in (1.1) and (1.2), shown at the bottom of the following page.

For simplicity of analysis, assume that $L_1 = L_2 = L$, $C_1 = C_2 = C$, and $R_1 = R_1 = R$. In case of no load ($r_L = \infty$), the

Manuscript received January 14, 2013; revised May 14, 2013; accepted May 21, 2013. Date of publication June 21, 2013; date of current version August 02, 2013. This work was supported in part by the National Science Foundation (NSF) under NSF CAREER Award (ECCS-0845849), EECS-1231957 and CCF-1162202, by the NSF directorate for Computer and Information Science and Engineering Computing Research Infrastructure (CISE CRI) under Grant CNS-1059289, by the Center for Design of Analog-Digital Integrated Circuits (CDADIC), and by the Korean Government under Contract NRF-2011-220-D00084.

The authors are with the School of Electrical Engineering and Computer Science (EECS), Washington State University, Pullman, WA 99163 USA (e-mail: dheo@eecs.wsu.edu).

Color versions of one or more of the figures in this paper are available online at http://ieeexplore.ieee.org.

Digital Object Identifier 10.1109/TMTT.2013.2267749

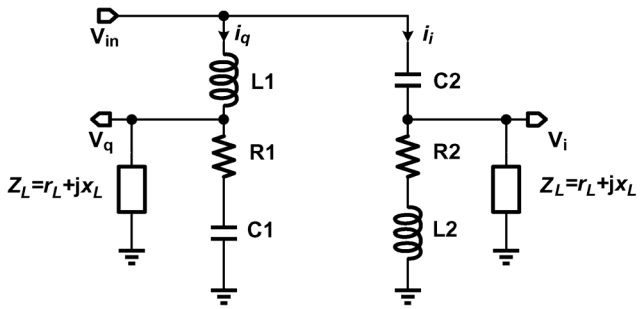

Fig. 2. Simple PPF.

functions $H_q(\omega)$ and $H_i(\omega)$ can be rewritten as follows:

$$H_q(\omega) = \frac{R - \frac{j}{\omega C}}{R - j\left(\frac{1}{\omega C} - \omega L\right)} \tag{2.1}$$

$$H_i(\omega) = \frac{R + j\omega L}{R - j\left(\frac{1}{\omega C} - \omega L\right)}. \tag{2.2}$$

The phase error ($\Phi_{\text{error\_ideal}} = |90 - |\angle H_i(\omega) - \angle H_q(\omega)||$) and amplitude error ($A_{\text{error\_ideal}} = |20\log(|H_i(\omega)|/|H_q(\omega))|$) can be defined as in [17] as follows:

$$\Phi_{\text{error\_ideal}}(\omega) = 90 - \tan^{-1}\left(\frac{1}{\omega CR}\right) - \tan^{-1}\left(\frac{\omega L}{R}\right)[^\circ] \tag{3.1}$$

$$A_{\text{error\_ideal}}(\omega) = \left|10\log\left(\frac{R^2+\omega^2L^2}{R^2+1/\omega^2C^2}\right)\right|[\text{dB}]. \tag{3.2}$$

It can be deduced from (3) that quadrature outputs are obtained at all frequencies if $Q = \sqrt{(L/C)}/R$ is chosen to be unity. However, amplitude mismatch increases as we move away from resonant frequency due to the inherent high- and low-pass nature of the circuit.

Now, let us take the case of a purely resistive load with finite resistance. Let

$$Z_{\text{denom}} = R(1 + Q^2\alpha) \tag{4.1}$$

where $\alpha = R/r_L$.

At frequencies close to $\omega_0 = 1/\sqrt{LC}$, we can then rewrite (1.1) and (1.2) as follows:

$$H_q(\omega) \approx \frac{R - j\frac{1}{\omega C}}{Z_{\text{denom}} + j\left(2 + \frac{R}{r_L}\right)\Delta Z + jQ\alpha R} \tag{5.1}$$

$$H_i(\omega) \approx \frac{R + j\omega L}{Z_{\text{denom}} + j\left(2 + \frac{R}{r_L}\right)\Delta Z - jQ\alpha R} \tag{5.2}$$

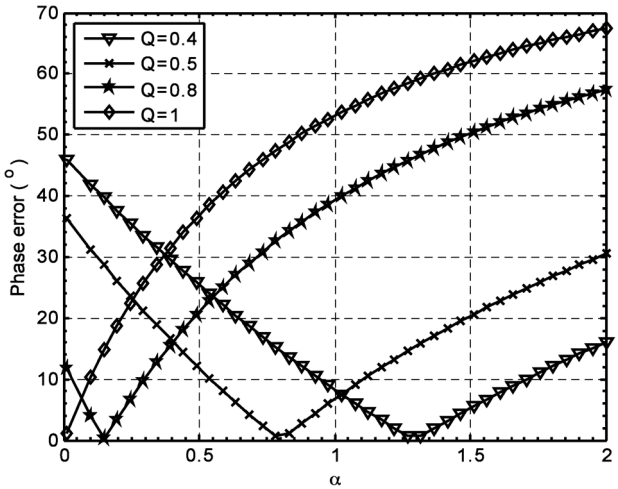

Fig. 3. Plot of phase error (6.1) versus α for different values of Q in the case when the PPF has purely resistive loading.

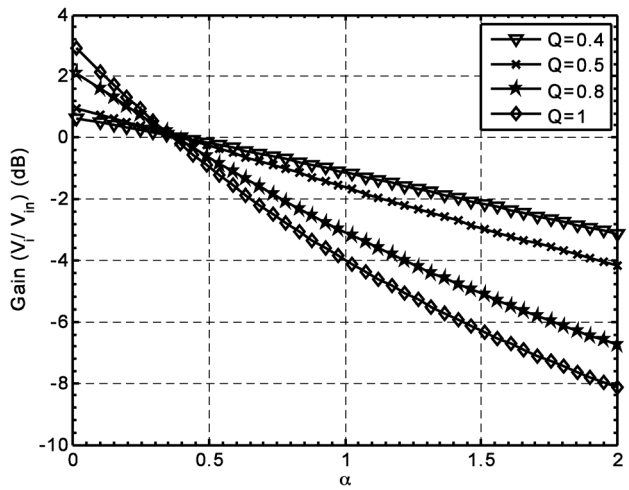

Fig. 4. Simulated output gain (5.2) versus α for different values of Q in the case when the PPF has purely resistive loading. The two quadrature outputs do not show any amplitude mismatch under purely resistive loading.

where $\Delta Z = \Delta\omega L \approx \Delta\omega/\omega_0^2 C$, $\omega = \omega_0 + \Delta\omega$. The phase error in this case can be written as follows:

$$\Phi_{\text{error},r_L} = \left|\Phi_{\text{error\_ideal}} - \tan^{-1}\left(\frac{2Q\alpha(1+Q^2\alpha)}{(1+Q^2\alpha)^2 - \alpha^2Q^2}\right)\right|[^\circ] \tag{6.1}$$

$$A_{\text{error},r_L}(\omega_0) = 0 \text{ dB}. \tag{6.2}$$

$$H_q(\omega) = \frac{R_1 + \frac{x_L}{\omega C_1 r_L} + j\left(\frac{R_1 x_L}{r_L} - \frac{1}{\omega C_1}\right)}{R_1 + \frac{L_1}{C_1 r_L} + \left(\frac{1}{\omega C_1} - \omega L_1\right)\frac{x_L}{r_L} + j\left[\frac{R_1 x_L}{r_L} - \left(\frac{1}{\omega C_1} - \omega L_1\right) + \frac{\omega L_1 R_1}{r_L}\right]} \tag{1.1}$$

$$H_i(\omega) = \frac{R_2 - \frac{\omega L_2 x_L}{r_L} + j\left(\frac{R_2 x_L}{r_L} + \omega L_2\right)}{R_2 + \frac{L_2}{C_2 r_L} + \left(\frac{1}{\omega C_2} - \omega L_2\right)\frac{x_L}{r_L} + j\left[\frac{R_2 x_L}{r_L} - \left(\frac{1}{\omega C_2} - \omega L_2\right) - \frac{R_2}{\omega C_2 r_L}\right]} \tag{1.2}$$

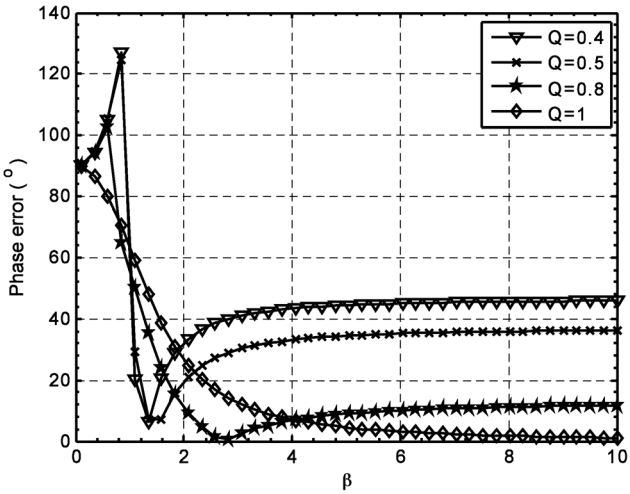

Fig. 5. Simulated quadrature phase error (7.1) versus β for different values of Q when the PPF has purely reactive loading.

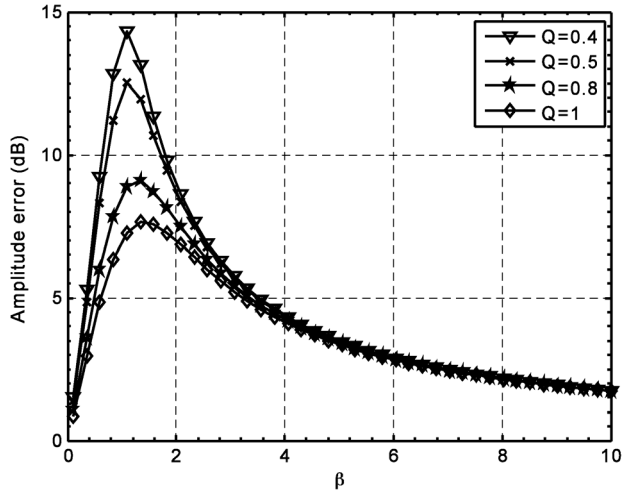

Fig. 6. Simulated amplitude error (7.2) versus β for different values of Q when the PPF has purely reactive loading.

Fig. 3 shows phase error versus $\alpha$for different values of Q. It can be seen that α needs to be less than 0.01 for phase error to settle within 10° when $Q = 1$, while the value of α needs to be in between 0.55 and 1.2 for the same phase error when Q is reduced to 0.5. However, with α increasing, output amplitude reduces, as can be seen from Fig. 4. Hence, to achieve a voltage gain, an extremely low α is desired. This would imply an extremely large output resistance. In the case of MOSFET designs, when a common gate buffer can provide a purely resistive impedance, this value of α would imply an extremely low g_m, and hence, would not be an effective buffer. Note that the amplitude error is always zero in this case in proximity of resonant frequency. With Q decreasing, the filter is more tolerant to variations in α as phase error is maintained low for a wide range of α.

In the case of a purely reactive load, the phase error at resonant frequency can be expressed as follows:

$$\Phi_{\text{error},b_L} = \left|\Phi_{\text{ideal\_error}} - \tan^{-1}\left(\frac{2Q}{Q^2+\beta^2-1}\right)\right| [^\circ] \quad (7.1)$$

$$A_{\text{error},b_L} = \left|10\log\left(\frac{Q^2+(\beta+1)^2}{Q^2+(\beta-1)^2}\right)\right| [\text{dB}] \quad (7.2)$$

where $\beta = L_L/L$ in case of inductive load ($x_L = \omega L_L$) and $\beta = C/C_L$ in case of capacitive load ($x_L = -1/\omega C_L$).

The phase error at output versus β with different Q values is shown in Fig. 5. It can be noted that β needs to be greater than 5 in order to achieve phase error within 5° for the case when Q is unity. However, when Q is decreased to 0.8, $\beta = 3$ gives low phase error. A large β is also desired to obtain small amplitude error, as seen in Fig. 6. Large β becomes impractical in the case of inductive load, due to the large size of load inductor required. β can be made large in the case of capacitive loading, meaning small loading capacitance. For capacitive loading due to output buffer devices, as in the case of a common gate buffer or a source follower, the size of the loading capacitor is governed by device sizes required for a given gain. Small input capacitance for a source follower would mean a small size device, and hence, high resistance at the output. This would, in turn, require impedance transformation for proper matching to the following stage. The size of filter capacitor C is also limited by the frequency of operation.

If capacitive only load is considered, the PPF in Fig. 2 reduces to the quadrature all-pass filter [17] when $Q = 1$. In this case, to maintain low phase error, a very small load capacitor is required (large β). This can be an issue when the design is meant for millimeter waves. When Q is reduced, the load capacitance can be increased to maintain lower phase error, as is evident from Fig. 5. A similar observation is made in [22].

In the case of a general loading ($Z_L = r_L + jx_L$), load quality factor ($Q_L = x_L/r_L$) can be defined. The phase and amplitude error at ω_0 in this case can be expressed as follows:

$$\Phi_{\text{error},Z_L} = \left|\Phi_{\text{error\_ideal}} - \tan^{-1}\left(\frac{2Q\alpha(1+Q^2\alpha)}{(1+Q^2\alpha)^2+Q_L^2-Q^2\alpha^2}\right)\right| [^\circ] \quad (8.1)$$

$$A_{\text{error},Z_L} = \left|10\log\left(\frac{1+\left[\frac{(Q_L+Q\alpha)}{(1+Q^2\alpha)}\right]^2}{1+\left[\frac{(Q_L-Q\alpha)}{(1+Q^2\alpha)}\right]^2}\right)\right| [\text{dB}]. \quad (8.2)$$

The dependence of Φ_{error,Z_L} with Q_L at $Q = 0.4$ is shown in Fig. 7. Equation (8) points to an important property of the PPF in Fig. 2. The effect of Q_L on Φ_{error,Z_L} for a given α is extremely minute if sufficiently low Q_L is chosen, as can be derived from (8.1). However, a low Q_L can drastically reduce the amplitude error, as is evident from Fig. 8. It can be seen that if Q of the network is sufficiently low, a small quality factor load can be used while maintaining low phase error. Hence, if $Q_L \ll Q\alpha$ and Q_L is chosen sufficiently small, low amplitude error can be maintained. The amplitude gain of the PPF with $Q = 0.4$ is shown in Fig. 9. When Q is reduced, a very low attenuation can easily be obtained for α larger than unity. It can also be observed that a larger gain is obtained with an inductive load.

The effects of loading condition on performance of PPF versus frequency are shown in Figs. 10 and 11. While a proper

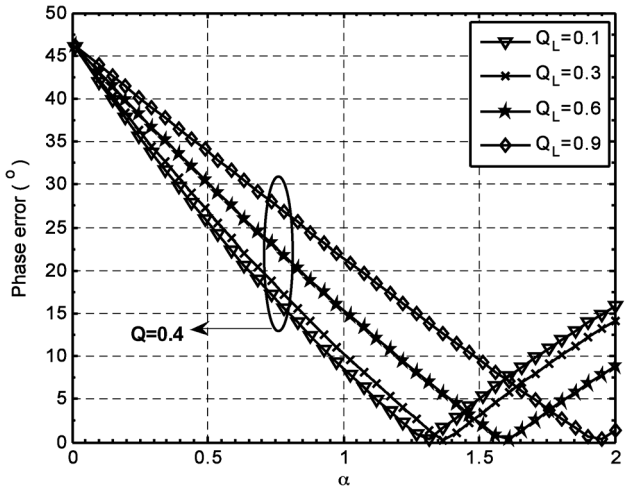

Fig. 7. Simulated quadrature phase error (8.1) versus α under load with varying quality factor at $Q = 0.4$.

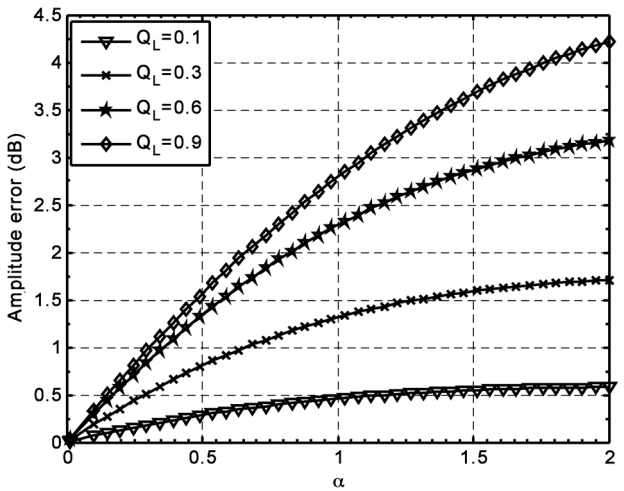

Fig. 8. Simulated quadrature amplitude error (8.2) versus α under load with varying quality factor at $Q = 0.4$.

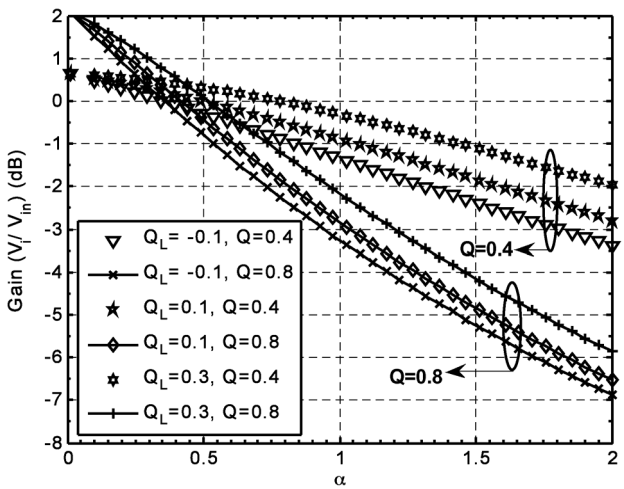

Fig. 9. Simulated gain of the PPF (1.1) versus α under load with varying Q_L and Q. A negative Q_L stands for capacitive load, while positive Q_L represents an inductive load.

choice of α results in very low phase error in all cases, loading conditions results in shift of effective ω_0 without any bandwidth advantages. This shift in ω_0 under capacitive loading is a well-known phenomenon [17].

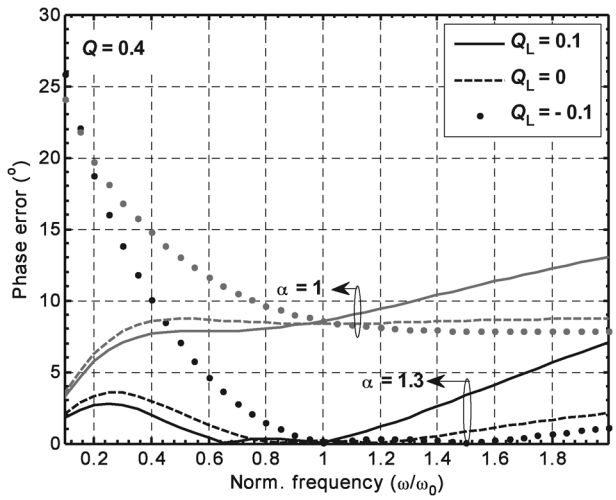

Fig. 10. Simulated phase error versus normalized frequency of the PPF for different loading conditions.

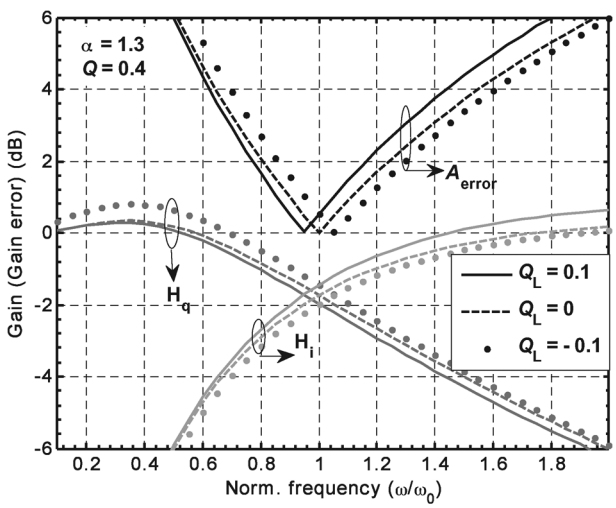

Fig. 11. Simulated gain and gain error versus frequency of the PPF at different loading conditions.

The results obtained in this section are very useful, as a low quality factor PPF can be implemented for a wide bandwidth without high loss in the quadrature filter. In addition, a low quality factor PPF would mean larger input impedance; thus, easy matching can be obtained independent of the phase error by the choice of proper α. A larger input impedance will also be a nonlimiting factor for linearity of the preceding stage [23], and hence, higher linearity can be obtained in an overall receiver chain. A quick look at Figs. 3 and 7 also points out that as a design step α can be selected first to satisfy the phase error requirement at a given Q of the PPF and the load quality factor, Q_L, then selected to satisfy the amplitude error requirement. As α can be made larger than unity, a small load resistance is required. In addition, a small Q_L can easily be obtained by a small size inductor. Since the value of Q_L can be low, an active inductor can be used to minimize area overhead. An example would be to use an active inductor buffer in heterobipolar transistor (HBT) based designs, as described in Section III.

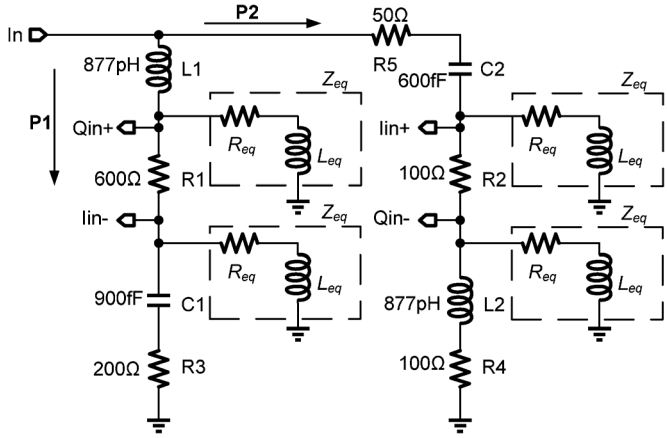

Fig. 12. Schematic of the wideband QPS with inductive load ($Z_{\rm eq}$).

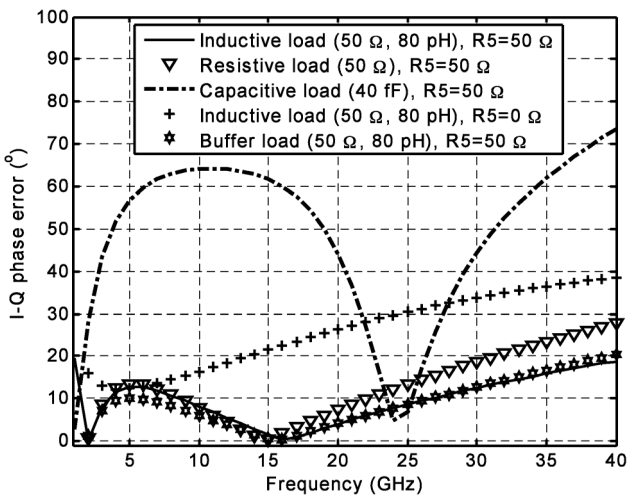

Fig. 13. Simulated dependence of phase error on the type of load in a QPS. An inductive load provides a wideband quadrature phase shift.

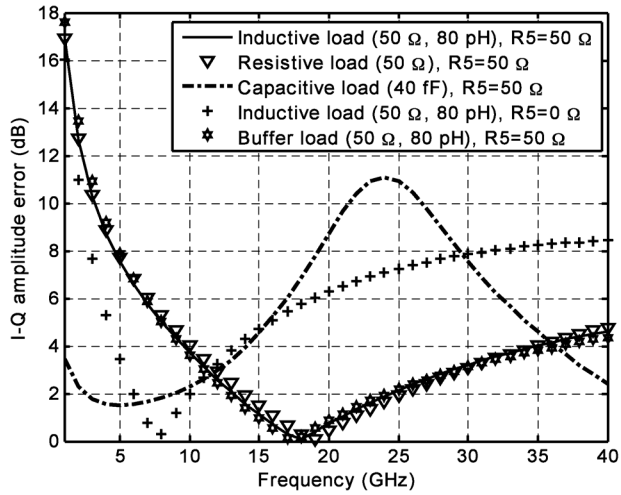

Fig. 14. Simulated dependence of amplitude error on the type of load in a QPS. An inductive load provides a low amplitude error over a wide bandwidth.

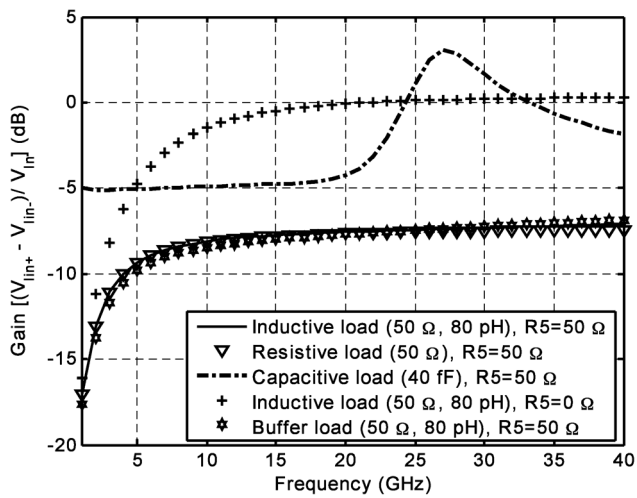

Fig. 15. Simulated in-phase gain versus frequency of the QPS for different types of load.

III. Proposed QPS

Based on the results derived in Section II, a wideband quadrature filter is implemented. The schematic of the proposed QPS is shown in Fig. 12. The filter consists of a high- and low-pass path in parallel. The quality factor of each path is degenerated by adding series resistors. Also, the resonant frequencies of each path are chosen slightly apart so as to create a wideband effect. Outputs of the filter are taken in a pseudo-differential manner across the central resistors. Note that the negative signal nodes (Iin$-$, Qin$-$) are heavily attenuated compared to the positive nodes (Iin$+$, Qin$+$). Hence, the effect of loading on the negative nodes can be ignored and results from Section II can still be applied to the proposed QPS.

The dependence of phase and amplitude error of the proposed QPS on different types of load is shown in Figs. 13 and 14, respectively. Circuit simulations for comparison are performed with ideal models for design elements.

The buffer is modeled as presented in the Appendix. It can be seen from Fig. 13 that capacitive loading is extremely narrowband in terms of phase-shifting bandwidth. A capacitive load of 40 fF is chosen to represent a practical loading device in the case of common emitter/collector (source/drain) buffer amplifiers. A resistive load shows a wideband phase-shifting behavior. When the load is made inductive, a further increase in phase-shifting bandwidth is achieved.

The voltage gain of the filter is shown in Fig. 15. The QPS with capacitive load is able to achieve low loss. However, the phase shift is narrow band. In the case of inductive and resistive load, the QPS has an attenuation of 7.5 dB. This loss can be easily compensated for by another gain stage in a receiver channel. The path $P2$ in Fig. 12 is loaded with a resistor $R5$. While $R5$ increases attenuation in the signal (Fig. 15), it makes quadrature phase shift more wideband. Both phase and amplitude errors are reduced by the addition of $R5$, as can be seen in Figs. 13 and 14.

IV. Circuit Implementation

To test the performance and application of the QPS, a phase shifter was implemented based on the vector sum approach. Phase shifts of desired resolution can be achieved by combining the prior quadrature shifted signals with desired weights. Hence, a vector modulator circuit consists of a variable gain block in each I–Q path, as well as some kind of sign selection to be able to produce phase shifts in any quadrant. Traditionally, a

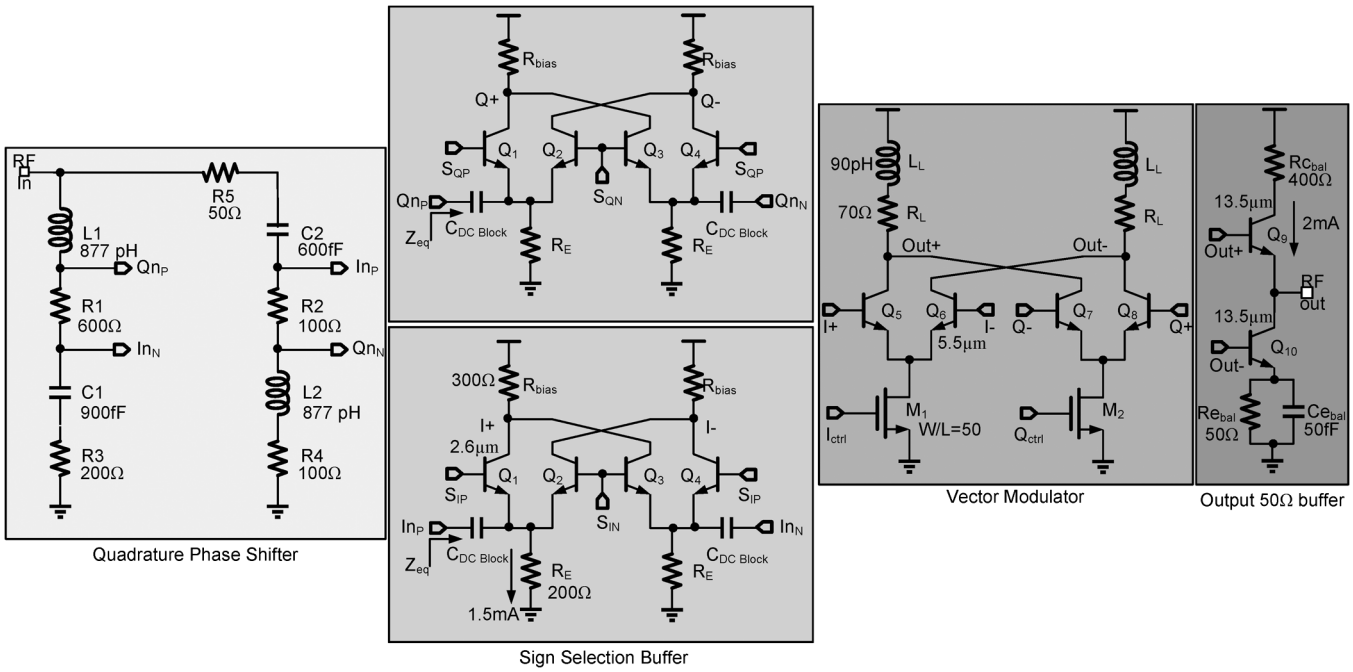

Fig. 16. Circuit schematics of the wideband phase shifter. The common-base sign selection buffers create inductive loading ($Z_{\rm eq}$) for the QPS. Bias circuits are not shown for clarity. $S_{\rm IP}$, $S_{\rm IN}$, S_{QP} and S_{QN} are ac ground nodes. Bias controls $I_{\rm ctrl}$ and $Q_{\rm ctrl}$ are provided using off-chip 2-bit DACs. The other two bits are used as digital controls for sign selection.

three-stack differential amplifier [16] is used in each path, and weighted I–Q outputs are current combined to generate the final desired phase [4], [16], [17], [20]. In a BiCMOS implementation of a variable gain amplifier (VGA) using bias current control, the input impedance is severely modulated due to the dependence of base–emitter diffusion capacitance on the bias current [16]. In addition, the input impedance of the VGA is capacitive. Since the QPS precedes the VGA, the change in input impedance induces significant error in quadrature generation. As the I–Q phase accuracy of the QPS determines the accuracy of the reference phases for further quantization, error in QPS needs to be minimized. Hence, it is desirable to buffer the QPS output before being fed to the VGA.

The proposed QPS is implemented with circuit components, as shown in Fig. 16. Path $P1$ is designed with a quality factor of 0.04, while path $P2$ is designed with a quality factor of 0.15. An extremely low Q in P1 helps to maintain low phase error over a wide bandwidth. The value of $(L1, C1)$ and $(L2, C2)$ pairs are chosen to obtain a resonant frequency of 6.26 GHz. After circuit optimization from SPECTRE, a load quality factor of 0.25 at 26 GHz is selected for this design. The load inductor size is chosen to resonate with the filter capacitor at 21 GHz.

A common base (CB) buffer provides a wideband impedance matching. In addition, as described in the Appendix, this buffer also provides an inductive load beneficial for quadrature phase shifting. Hence, a CB buffer topology is selected for this design. A typical CB buffer shows about 50 % variation in quality factor due to change in input resistance over the desired frequency range, as seen from Fig. 23. Since the load quality factor is small, the variation of load quality factor with frequency in the case of a CB buffer has a minimal impact on the proposed QPS performance.

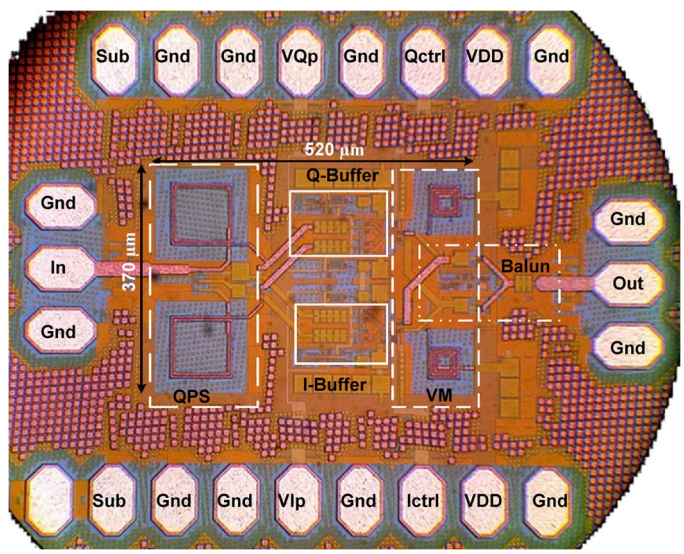

Fig. 17. Die micrograph of the proposed wideband phase shifter (active area: 520 μm × 370 μm).

To efficiently minimize the power overhead due to the CB buffer, additional functionality of sign selection logic is added to the buffer, as shown in Fig. 16. Bias voltages $S_{\rm IP}$ and $S_{\rm IN}$ are complementary in nature. Hence, transistor pairs (Q_1, Q_2) and (Q_3, Q_4) are ON complementarily, thus buffering either $\rm In_P - In_N$ or reversing the sign at the output. All of the transistors $Q_{1\text{-}4}$ are the same size. It is important to note that neither the output impedance, nor the input impedance is changed due to switching, and hence, quadrature phase error at the input is minimized due to sign switching.

Once the quadrature vectors are assigned, desired quadrants by selecting the signs of I and Q signals, these signals

TABLE I
QPS PERFORMANCE SUMMARY

Quantity	Measured Results
Technology	0.18 µm BiCMOS
Frequency band	15-35 GHz
Fractional BW	87 %
Input return loss	> 10
Max. phase error	2.98° @ 15 GHz
	6.39° @ 35 GHz
Max. amplitude error	< 2 dB
Power Consumption	10.8 mW (I_{DC}=6 mA, V_{DC}=1.8 V)*

* Power consumption of the CB buffer

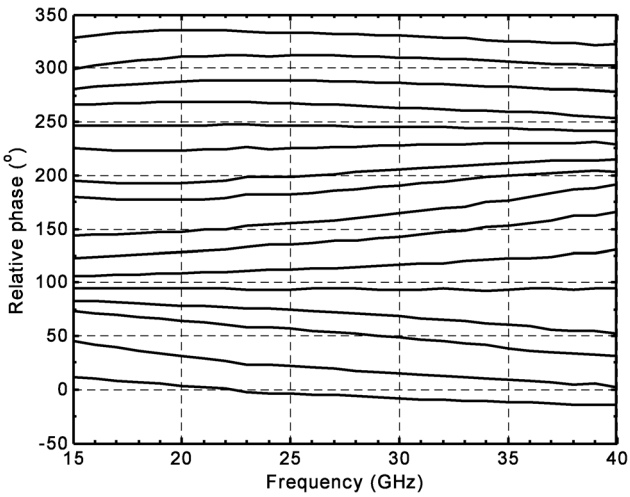

Fig. 18. Measured 16 relative phase states of the phase shifter.

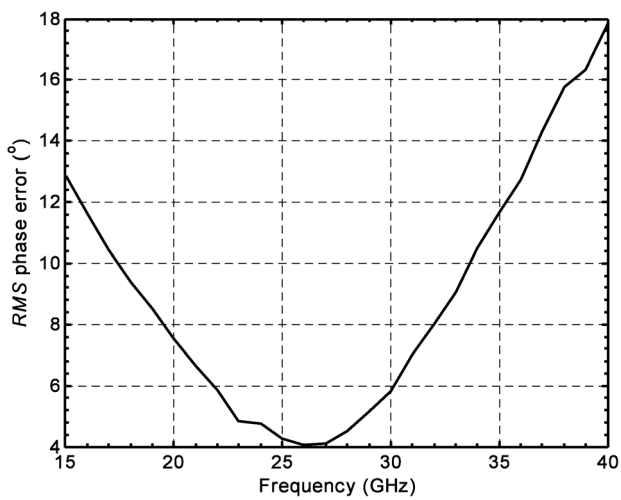

Fig. 19. Measured rms phase error of the proposed phase shifter.

are weighted and added in the vector modulator, as shown in Fig. 16. Q_5 and Q_6 with current source M_1 form the differential pair for I signals, while Q_7 and Q_8 with current source M_2 is used as an amplifier for Q signals. The currents from these amplifiers are added at the inductively peaked load due to L_L and R_L. Bias voltages $I_{\rm ctrl}$ and $Q_{\rm ctrl}$ are used to control the gain in each amplifier.

The QPS was implemented with $L1 = L2 = 877$ pH ($Q_{\rm ind} = 21$ at 26 GHz and self-resonant frequency = 50.9 GHz), $C1 = 900$ fF, $C2 = 600$ fF, $R1 = 600\ \Omega$, $R2 = 100\ \Omega$, $R3 = 200\ \Omega$, $R4 = 100\ \Omega$, and $R5 = 50\ \Omega$. The buffer is designed to provide a load with an inductance of $L_{\rm eq} = 80$ pH and $R_{\rm eq} = 30\ \Omega$.

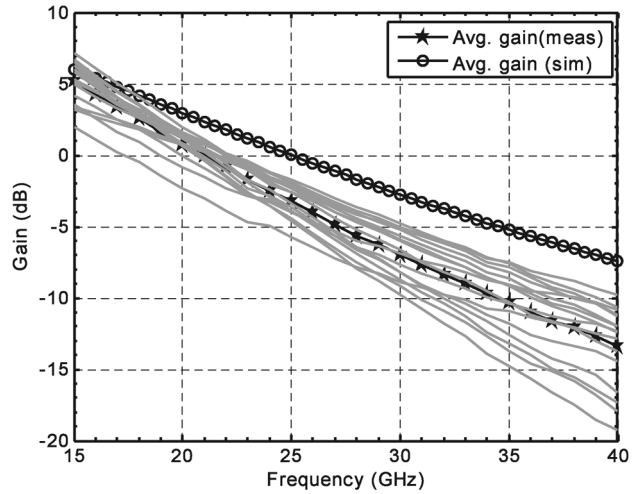

Fig. 20. Measured versus simulated gain variation over phase states of the phase shifter.

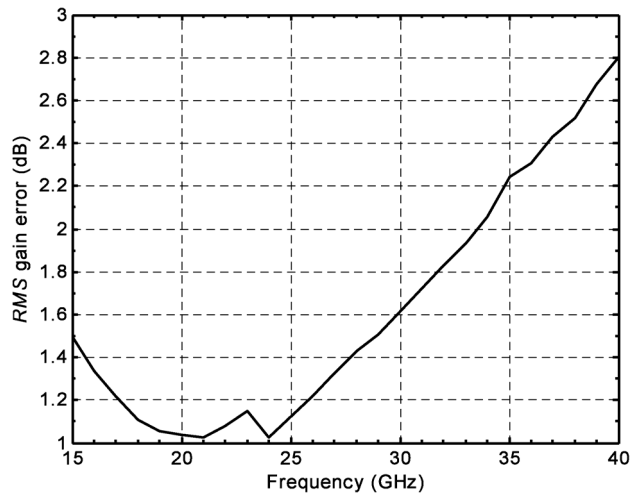

Fig. 21. Measured rms gain error of the phase shifter.

V. MEASUREMENT RESULTS

The proposed wideband phase shifter has been implemented in the TowerJazz 1P6M 0.18-μm BiCMOS process with f_T of 150 GHz and occupies an area of 0.19 mm^2. The chip micrograph of the phase shifter is shown in Fig. 17. Passives and RF interconnects have been simulated in ADS Momentum. For test purposes, differential outputs of the phase shifter are converted to single-ended output using an active balun. The active balun is also designed to drive a 50-Ω load. The phase shifter consumes a current of 14 mA, while the balun consumes 2 mA from a 1.8-V supply.

The input of the QPS is well matched to 50 Ω and the input reflection coefficient is below -10 dB from 5 to 35 GHz. The QPS can be characterized by measuring the phase shifter output with only the I-path or Q-path activated. When done so, the QPS has a maximum phase error of 2.98° at 15 GHz and 6.39° at 35 GHz with a minimum at 20 GHz. The amplitude error remains within 2 dB with maximum occurring at 35 GHz and

TABLE II
PERFORMANCE COMPARISON OF THE PHASE SHIFTER

Ref.	[3]	[12]	[16]	[17]	[22]	**This work**
Tech.	0.18 μm CMOS	0.18 μm BiCMOS	0.18 μm BiCMOS	0.13 μm CMOS	0.13 μm BiCMOS	**0.18 μm BiCMOS**
Type	PVS[2]	Switched LC	VS[1]	VS[1]	VS[1]	**VS[1]**
Freq. (GHz)	22–26	34–39	30–50	15–26	60–78	**15–35**
Fractional BW	17 %	14 %	52 %	56 %	26%	**87 %**
Phase Res.	22.5°	11.25°	22.5°	22.5°	22.5°	**22.5°**
VDD (V)	1.8	1.8	5	1.5	3	**1.8**
Power (mW)	0	0	40	11.7	34.8	**25.2[5]**
Phase error (*rms*)	1.5°	< 12°	7–8.8°	6.5–16°	<9.1°	**4.2–13°**
Gain error (*rms*) (dB)	0.8	< 0.9	1.2	1.1–2.1	<1.3	**1–2.2**
Absolute Gain (dB)	-15.3	-13.6	7.5	-4.6– -3	-3.2	**5– -13.5**
Input P1dB (dBm)	12	8.7	-5[3]	-0.8	N/A	**-6.25**
Chip area	0.31	N/A	N/A[4]	0.14	N/A	**0.19**

[1] Vector sum (VS), [2] Passive vector sum (PVS), [3] Estimated from simulation, [4] Not available, [5] Does not include active balun.

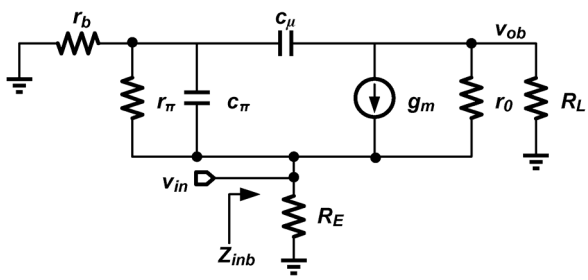

Fig. 22. Small-signal model of a CB buffer.

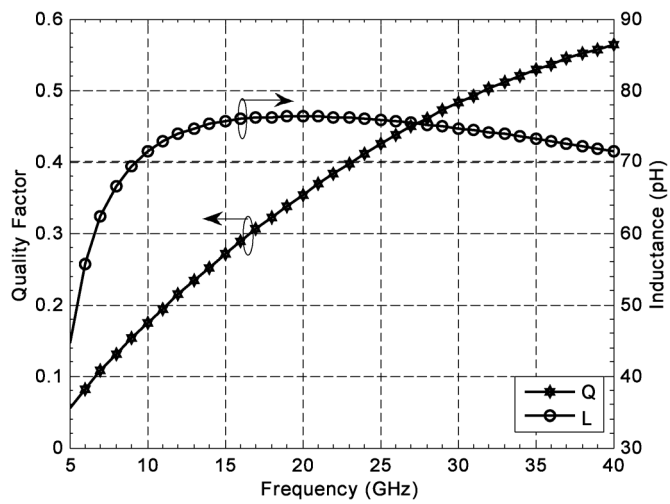

Fig. 23. Simulated quality factor and inductance obtained using a common-base buffer. $g_m = 41$ mS, $R_E = 200\ \Omega$, $r_b = 144\ \Omega$, and $c_\pi = 40$ fF.

minimum at 20 GHz. The amplitude error at 15 GHz is 1.44 dB. Table I summarizes the measured results of the QPS.

The phase shifter was measured using Agilent Technologies' PNA-X Microwave Network Analyzer. Standard short-open-load-thru (SOLT) calibration was carried out to cancel probe and connecting cable losses. The 16 measured relative phase states and the rms phase error of the phase shifter are shown in Figs. 18 and 19, respectively. The rms phase error of the phase shifter is 4.2°–13° from 15 to 35 GHz. The gain variation over phase states of the phase shifter and the rms gain error are shown in Figs. 20 and 21, respectively. The phase shifter shows an average gain from 5 to −13.5 dB, while the rms gain error is 1–2.2 dB from 15 to 35 GHz. The measured gain slope is larger than simulated. This might be due to inaccurate electromagnetic (EM) simulation and larger balun loss at higher frequencies. The gain slope seen at the output of the phase shifter can be easily compensated with another gain stage peaked at high frequency in a phase array. Hence, the design is focused on attaining high phase accuracy rather than gain flatness. The phase shifter shows a measured input P1 dB of -6.25 ± 0.75 dBm across the frequency range of 15–40 GHz.

Table II presents the performance comparison of the proposed phase shifter with the proposed QPS to current state-of-the-art RF phase shifters. The design in [3] and [12] are passive implementations and suffers from both bandwidth and high insertion loss. The design in [17] is based on CMOS and is able to achieve a very low power operation and a wideband phase accuracy. The wide phase-shifting bandwidth (bandwidth in which the phase shifter has acceptable phase and gain error) can be attributed to lower impedance modulation in CMOS compared to an HBT with the same change in bias current [16]. In the BiCMOS design of [16], the authors apply a similar approach as in [17], but this approach suffers from very high supply voltage due to multi-stack implementation. As can be seen from the table, the proposed design achieves the widest phase-shifting bandwidth with low phase error and low gain error. The proposed phase shifter operates from a 1.8-V power supply, as device stacking in the vector modulator is avoided.

VI. CONCLUSION

A Ku-, K-, and Ka-band (15–35 GHz) phase shifter implemented in a 0.18-μm BiCMOS process has been presented in this paper. An analysis of a simple PPF under different load conditions shows that a low quality factor inductive load is most suitable for wideband operation through low Q PPFs. Based on the analysis, a novel inductive load single-ended input PPF is used for high I/Q accuracy wideband quadrature generation. The QPS so designed is embedded into a low power vector sum phase shifter. Sign selection and vector combining is implemented in two stages to enable low-voltage operation without compromising linearity. Measurement results show that the phase shifter achieves an 87% phase-shifting fractional

bandwidth while maintaining gain error less than 2.2 dB. The ultra wide-bandwidth coupled with low-power operation makes the phase shifter most suitable for on-chip integration with wideband RF phase-shifting phased arrays.

APPENDIX

A. Active Inductor Buffer

An inductive load can be implemented by common-base buffer amplifiers due to the presence of large intrinsic base resistance in an HBT. Active inductance has been achieved in CMOS by the use of a series resistance at the gate [24], [25]. The following analysis presents a derivation of the active inductance that can be achieved in the case of an HBT design for the sake of completeness. The small-signal model of a common-base buffer is shown in Fig. 22.

The input impedance $(Z_{\rm inb})$ of a CB buffer can be written as in (9.1). The effect of c_μ is ignored as base–collector gain is small, and hence, the Miller effect is not prominent,

$$Z_{\rm inb} = \frac{1}{g_m} \cdot \frac{1 + sr_b c_\pi}{(1 + sc_\pi/g_m) + \left(\frac{1}{g_m R_E}\right)(1 + sr_b c_\pi)} \quad (9.1)$$

where g_m is the device transconductance, r_b is the base resistance, $s = j\omega$, R_E is the resistance due to current source at the emitter, and c_π is the base–emitter capacitance. The equivalent inductance $(L_{\rm eq})$ at the input of the CB buffer for a given frequency (ω) can be derived from (9.1) as in (9.2) as follows:

$$\begin{aligned} L_{\rm eq} &= \frac{1}{\omega_t} \cdot \frac{(r_b - 1/g_m)}{(1 + 1/g_m R_E)^2 + \left(\frac{\omega}{\omega_t}\right)^2 (1 + r_b/R_E)^2} \\ &= \frac{1}{\omega_t} \cdot \frac{(r_b - 1/g_m)}{(1 + 1/g_m R_E)^2}, \qquad \text{for } \omega \ll \omega_t \end{aligned} \quad (9.2)$$

where $\omega_t = g_m/c_\pi$ is the unity gain (current) frequency of the device. Note that in both (9.1) and (9.2), the effect of base–emitter resistance (r_π) is ignored. This assumption is valid at frequencies of our interest, as c_π dominates r_π. The resistive part of the input impedance can be written as

$$r_L = \frac{1}{g_m} \cdot \frac{1 + 1/g_m R_E + \left(\frac{\omega}{\omega_t}\right)^2 g_m r_b (1 + r_b/R_E)}{(1 + 1/g_m R_E)^2 + \left(\frac{\omega}{\omega_t}\right)^2 (1 + r_b/R_E)^2}. \quad (9.3)$$

Equation (9.3) points to the fact that r_L is approximately $1/g_m$ at dc. However, r_L increases with frequency. With proper choice of g_m, R_E and the device size, Q_L of about 0.4 can be easily obtained. For example, $L_{\rm eq} = 76$ pH and $Q_L = 0.44$ can be obtained at 26 GHz when $g_m = 41$ mS, $r_b = 144\ \Omega$, $c_\pi = 40$ fF, and $R_E = 200\ \Omega$ is chosen. Fig. 23 shows the quality factor and inductance values obtained using the aforementioned parameters. These values are easily obtained in an 0.18-μm SiGe BiCMOS process using a device with emitter area of $0.2 \times 2.64\ \mu{\rm m}^2$ and a bias current of 1 mA.

ACKNOWLEDGMENT

The authors thank Dr. A. Kar-Roy and TowerJazz for chip fabrication, and members of the Center for Design of Analog–Digital Integrated Circuits (CDADIC) for their support.

REFERENCES

[1] S. Shekhar, J. S. Walling, and D. J. Allstot, "Bandwidth extension techniques for CMOS amplifiers," *IEEE J. Solid-State Circuits*, vol. 41, no. 11, pp. 2424–2439, Nov. 2006.

[2] H. R. Fang, X. Tang, K. Mouthaan, and R. Guinvarc'h, "180 ° and 90 ° reflection-type phase shifters using over-coupled lange couplers," *IEEE Trans. Microw. Theory Techn.*, vol. 60, no. 11, pp. 3440–3448, Nov. 2012.

[3] C.-W. Wang, H.-S. Wu, and C.-K. C. Tzuang, "CMOS passive phase shifter with group-delay deviation of 6.3 ps at K-band," *IEEE Trans. Microw. Theory Techn.*, vol. 59, no. 7, pp. 1778–1786, Jul. 2011.

[4] A. Valdes-Garcia, S. T. Nicolson, J.-W. Lai, A. Natarajan, P.-Y. Chen, S. K. Reynolds, J.-H. C. Zhan, D. G. Kam, D. Liu, and B. Floyd, "A fully integrated 16-element phased-array transmitter in SiGe BiCMOS for 60-GHz communications," *IEEE J. Solid-State Circuits*, vol. 45, no. 12, pp. 2757–2773, Dec. 2010.

[5] M.-D. Tsai and A. Natarajan, "60 GHz passive and active RF-path phase shifters in silicon," in *IEEE RFIC Symp. Dig.*, Jun. 2009, pp. 223–226.

[6] S. J. Kim and N. H. Myung, "A new active phase shifter using a vector sum method," *IEEE Microw. Guided Wave Lett.*, vol. 10, no. 6, pp. 233–235, Jun. 2000.

[7] P.-S. Huang and H.-C. Lu, "Improvement of the phase shifter in 90 power splitter for NWB applications," *IEEE Microw. Wireless Compon. Lett.*, vol. 22, no. 12, pp. 621–623, Dec. 2012.

[8] F. Ellinger, R. Vogt, and W. Bachtold, "Ultracompact reflective-type phase shifter MMIC at C-band with 360 ° phase-control range for smart antenna combining," *IEEE J. Solid-State Circuits*, vol. 37, no. 4, pp. 481–486, Apr. 2002.

[9] M. Meghdadi, M. Azizi, M. Kiani, A. Medi, and M. Atarodi, "A 6-Bit CMOS phase shifter for S-band," *IEEE Trans. Microw. Theory Techn.*, vol. 58, no. 12, pp. 3519–3526, Dec. 2010.

[10] L. Wang, P. Sun, Y. You, A. Mikul, R. Bonebright, G. A. Kromholtz, and D. Heo, "Highly linear Ku-band SiGe PIN diode phase shifter in standard SiGe BiCMOS process," *IEEE Microw. Wireless Compon. Lett.*, vol. 20, no. 1, pp. 37–39, Jan. 2010.

[11] J. G. Yang and K. Yang, "Ka-band 5-bit MMIC phase shifter using InGaAs PIN switching diodes," *IEEE Microw. Wireless Compon. Lett.*, vol. 21, no. 3, pp. 151–153, Mar. 2011.

[12] D.-W. Kang, J.-G. Kim, B.-W. Min, and G. M. Rebeiz, "Single and four-element Ka-band transmit/receive phased-array silicon RFICs with 5-bit amplitude and phase control," *IEEE Trans. Microw. Theory Techn.*, vol. 57, no. 12, pp. 3534–3543, Dec. 2009.

[13] H. Zarei and D. J. Allstot, "A low-loss phase shifter in 180 nm CMOS for multiple-antenna receivers," in *IEEE Int. Solid-State Circuits Conf. Tech. Dig.*, 2004, pp. 392–534.

[14] M. Parlak and J. F. Buckwalter, "A low-power, W-band phase shifter in a 0.12 μm SiGe BiCMOS process," *IEEE Microw. Wireless Compon. Lett.*, vol. 20, no. 11, pp. 631–633, Nov. 2010.

[15] Y.-Y. Huang, H. Jeon, Y. Yoon, W. Woo, C.-H. Lee, and J. S. Kenney, "An ultra-compact, linearly-controlled variable phase shifter designed with a novel *RC* poly-phase filter," *IEEE Trans. Microw. Theory Techn.*, vol. 60, no. 2, pp. 301–310, Feb. 2012.

[16] K.-J. Koh and G. M. Rebeiz, "A Q-band 4-element phased-array front-end receiver with integrated Wilkinson power combiners in 0.18 μm–SiGe BiCMOS technology," *IEEE Trans. Microw. Theory Techn.*, vol. 56, no. 9, pp. 2046–2053, Sep. 2008.

[17] K.-J. Koh and G. M. Rebeiz, "0.13-μm CMOS phase shifters for X-, Ku-, and K-band phased arrays," *IEEE J. Solid-State Circuits*, vol. 42, no. 1, pp. 2535–2546, Nov. 2007.

[18] X. Tang and K. Mouthaan, "Design of large bandwidth phase shifters using common mode all-pass networks," *IEEE Microw. Wireless Compon. Lett.*, vol. 22, no. 2, pp. 55–57, Feb. 2012.

[19] J. Kaukovuori, K. Stadius, J. Ryynanen, and K. Halonen, "Analysis and design of passive polyphase filters," *IEEE Trans. Circuits Syst. I, Reg. Papers*, vol. 55, no. 10, pp. 3023–3037, Nov. 2008.

[20] A. Asoodeh and M. Atarodi, "A Full 360 ° vector-sum phase shifter with very low RMS phase error over a wide bandwidth," *IEEE Trans. Microw. Theory Techn.*, vol. 60, no. 6, pp. 1626–1634, Jun. 2012.

[21] K. Miyaguchi, M. Hieda, M. Hangai, T. Nishino, N. Yunoue, Y. Sasaki, and M. Miyazaki, "An ultra compact C-band 5-bit MMIC phase shifter based on all-pass network," in *Proc. Eur. Microw. Integr. Circuits Conf.*, Sep. 2006, pp. 277–280.

[22] S. Y. Kim, D.-W. Kang, K.-J. Koh, and G. M. Rebeiz, "An improved wideband all-pass I/Q network for millimeter-wave phase shifters," *IEEE Trans. Microw. Theory Techn.*, vol. 60, no. 11, pp. 3431–3439, Nov. 2012.
[23] D.-W. Kang, K.-J. Koh, and G. M. Rebeiz, "A Ku-band two-antenna four-simultaneous beams SiGe BiCMOS phased array receiver," *IEEE Trans. Microw. Theory Techn.*, vol. 58, no. 4, pp. 771–780, Apr. 2010.
[24] T. H. Lee, *The Design of CMOS Radio-Frequency Integrated Circuits*. Cambridge, U.K.: Cambridge Univ. Press, 2004.
[25] I. E. Ho and R. L. Van Tuyl, "Inductorless monolithic microwave amplifiers with directly cascaded cells," in *IEEE MTT-S Int. Microw. Symp. Dig.*, May 1990, vol. 1, pp. 515–518.

Suman P. Sah (S'10) received the Bachelor of Technology (with honors) and Master of Technology degrees in electrical engineering from the Indian Institute of Technology Kharagpur, India, in 2009, and is currently working toward the Ph.D. degree at Washington State University, Pullman, WA, USA.

From February to June 2012, he was an Intern with Broadcom, Irvine, CA, USA, where he was involved with the design of a test for complex radio systems and ON-wafer testing and verification of high-frequency analog circuits. His research interests include design of signal generation circuits, high-frequency phased arrays, and millimeter-wave circuit design.

Xinmin Yu (S'10) received the B.S. degree in electrical engineering from Zhejiang University, Hangzhou, Zhejiang, China, in 2002, the M.S. degree in electrical engineering from the Beijing University of Posts and Telecommunications, Beijing, China, in 2006, and is currently working toward the Ph.D. degree at Washington State University, Pullman, WA, USA.

From May to August 2013, he was an Intern with Qualcomm Technologies Inc., San Diego, CA, USA, where he was involved with RF integrated circuit (RFIC) designs for cellular applications. His research focuses on RF and analog integrated circuit (IC) design, including wideband transceiver circuits in millimeter-wave band for wireless network-on-chip application, as well as low-power wireless transceivers for sensor network and biomedical applications.

Deukhyoun Heo (S'97–M'00–SM'13) received the B.S.E.E. degree in electrical engineering from Kyoungpuk National University, Daegu, Korea, in 1989, the M.S.E.E. degree in electrical engineering from the Pohang University of Science and Technology (POSTECH), Pohang, Korea, in 1997, and the Ph.D. degree in electrical and computer engineering from the Georgia Institute of Technology, Atlanta, GA, USA, in 2000.

In 2000, he joined the National Semiconductor Corporation, where he was a Senior Design Engineer involved in the development of silicon RF integrated circuits (RFICs) for cellular applications. Since Fall 2003, he has been an Associate Professor with the Electrical Engineering and Computer Science Department, Washington State University, Pullman, WA, USA. He has authored or coauthored approximately 100 publications, including peer-reviewed journal and international conference papers. He has primarily been interested in RF/microwave/opto-transceiver design based on CMOS, SiGe BiCMOS, and GaAs technologies for wireless and wireline data communications, batteryless wireless sensors and intelligent power management system for sustainable energy sources, adaptive beam formers for phased-array communications, and low-power high data-rate wireless links for biomedical applications.

Dr. Heo has served as an associate editor for the IEEE TRANSACTIONS ON CIRCUITS AND SYSTEMS—PART II: EXPRESS BRIEFS (2007–2009) and as an associate editor for the IEEE TRANSACTIONS ON MICROWAVE THEORY AND TECHNIQUES. He was the recipient of the 2000 Best Student Paper Award presented at the IEEE Microwave Theory and Techniques Society (IEEE MTT-S) International Microwave Symposium (IMS) and the 2009 National Science Foundation (NSF) CAREER Award.